Comparison of Iron-related MR Susceptibility and Transverse Relaxation Rates in the P19 Cell Model

Linshan Liu[1,2], Neil Gelman[1,2], Rebecca McGirr[1], R. Terry Thompson[1,2], Frank S Prato[1,2], Lisa Hoffman[1,2], and Donna E Goldhawk[1,2]
[1]*Imaging program, Lawson Health Research Institute, London, Ontario, Canada,* [2]*Medical Biophysics, Western University, London, Ontario, Canada*

TARGET AUDIENCE: Researchers and clinicians interested in using MRI for cell tracking**.**

INTRODUCTION: MRI-based cell tracking techniques (cellular MRI) play an important role in developing cellular therapy[1]. Localization of iron-labeled cells (e.g. with SPIO[2] or by genetic-modifications such as MagA expression[3]) is typically based on the influence of iron on the transverse relaxation rates (R2*, R2, R2' = R2* - R2) or on the magnetic susceptibility of the cells. Measurement of these MRI parameters in cells in vitro (*i.e.*, within a phantom) along with measurements of iron levels provides a means to compare the influence of iron loading on these parameters. In this abstract, we present and compare the correlation of each of these parameters to iron levels in P19 cells cultured in the presence and absence of iron supplementation. Note that the P19 cell model is derived from a mouse embryonic carcinoma and retains the capacity to differentiate into the three germ cell layers: endoderm, mesoderm and ectoderm.

MATERIALS & METHODS:

Cells. Four groups of P19 cells were used in this study: un-transfected parental control (P) and MagA-expressing (M), cultured in the presence and absence of iron supplementation (250 µM ferric nitrate). After 7 days, cells were harvested, washed with phosphate buffered saline pH 7.4 and centrifuged at 400 x g in custom made Ultem wells (diameter ~ 6mm) for MRI. Alternatively, washed cells were lysed in RIPA buffer using sonication, quantified with the BCA protein assay, and analyzed by inductively coupled plasma mass spectrometry (ICP-MS) to measure cellular iron content.

Phantoms. To minimize macroscopic B0 inhomogeneity, sample wells were embedded in a 9cm spherical phantom filled with 4% gelatin (Fig 1). Samples P, P+Fe, M and M+Fe are numbered 1 to 4, respectively. A plastic peg provided orientation.

MRI. Phantoms were scanned at 3T. To acquire T2*-wieghted images, multi-echo GRE was used (TE= 6.12, 14.64, 23.16, 31.68, 40.2, 50, 60, 70 and 79.9 ms; TR = 2000 ms). To acquire T2-weighted images, single echo SE was conducted (TE=13, 30, 40, 60, 80, 100, 150, 200 and 300 ms; TR= 2000ms). A single slice (1.5mm thickness) located at the centre of the well was acquired; in-plane resolution is 0.6×0.6 mm^2.

Generating Δf_0 map. To remove the constant phase term, we calculated the Hermitian product (HP) between the first and the later echoes. To remove phase wraps, we performed phase unwrapping[4] to the HP phase image for each echo. To generate ΔB_0 frequency map at each echo, we scaled the unwrapped phase image by a factor of $(1/2\pi\Delta TE)$, where ΔTE is the echo time difference between the first and the later echoes. To generate the final echo-combined Δf_0 map (Fig 1a), we calculated the algorithmic mean over all echoes.

Calculating susceptibility. To calculate an apparent value of susceptibility (χ_a), we first identified the center of a well and then drew a circle (diameter 18 pixels) from the ΔB_0 map (e.g., Fig. 1a and 1c). We defined χ_a (ppm) as the difference of mean frequency values between the five highest (positive) and lowest (negative) pixels inside the circle, but outside the well, divided by Larmor frequency. Note the definition of χ_a is based on an infinite cylinder model[6].

Generating R2*, R2 and R2' maps. To estimate R2* and R2, we fit the signal intensity vs. TE using a 2-parameter mono-exponential function on a pixel-by-pixel basis. The R2' map was derived as the difference between R2* and R2 maps. To represent the corresponding values for each well (mean values of R2*, R2 and R2'), we drew a region of interest for each well on the image including voxels in the well but excluding voxels close to the wall.

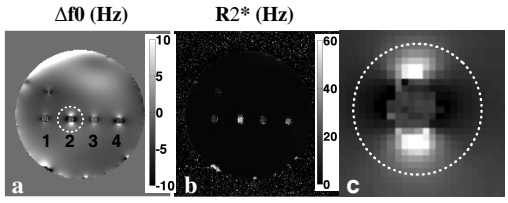

Figure 1. Gelatin Phantom. Sample wells are shown in axial cross section: (a) frequency map, (b) R2* map, and (c) enlarged region of interest (ROI) from sample 2 in panel (a). Apparent susceptibility was determined from the ROI. Samples 2 and 4 are iron-supplemented cells; samples 1 and 3 are un-supplemented.

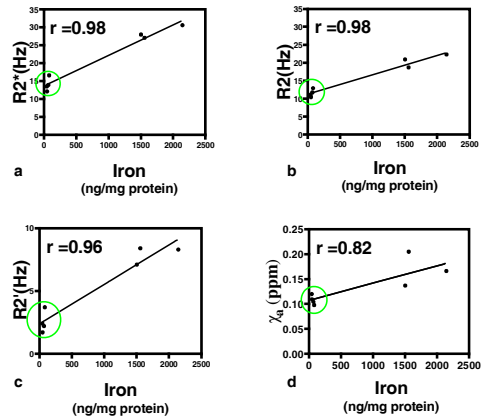

Figure 2. Comparison of Transverse Relaxation Rates and Apparent Susceptibility Versus Cellular Iron Content. P19 cells were cultured in the presence and absence of iron supplementation, mounted in a gelatin phantom and scanned at 3T. Plots show a linear regression analysis of (a) R2, (b) R2*, (c) R2' and (d) χ_a vs. cellular iron content. Symbols included in green circles correspond to cells without iron supplementation. For a,b,c, $p< 0.001$; for d, $p<0.05$

RESULTS & DISCUSSION: As expected, more visible local frequency spatial variations (Fig 1a) as well as larger R2* values (Fig 1b) are observed for iron-supplemented cells, in contrast to un-supplemented samples. As indicated in Fig 2 correlations of the relaxation rates (R2*, R2, R2'), with iron content, for this limited number of samples, are stronger than the correlation of χ_a with iron content. A previous study of human tumor cell line[7], involving only the relaxation rates found similarly strong correlations with iron content. In-vivo R2, and hence also R2*, are believed to be more sensitive to tissue properties unrelated to iron content (i.e. less iron specificity) than R2'[6]. The potential for specificity is also consistent with the small iron independent contribution to R2' (y-intercept in Fig. 2c) relative to the iron-related change in R2' from lowest to highest iron content.

CONCLUSION: Although estimation of apparent susceptibility correlates with cellular iron contrast, the transverse relaxation rates show stronger association with iron content in samples of P19 cells.

REFERENCES: [1] Hoffman and Gambhir, Radiology 44: 39-47, 2007. [2] Heyn et al., MRM 53:312-320, 2005. [3] Goldawk, et al., Nanomed and Nanobiotech 4:378-388, 2012. [4] Liu and Drangova, MRM 68: 1303-1316, 2012. [5] Chu et al., MRM 13:239-262, 1990.[6] Gelman, et al., Neuroradiology, 759–767,1999. [7] Sengupta, Master Thesis, Western University, 2014.